

Mass and Information Feedbacks through Receptor Endocytosis Govern Insulin Signaling as Revealed Using a Parameter-free Modeling Framework^{*[5]}

Received for publication, January 22, 2010, and in revised form, April 19, 2010. Published, JBC Papers in Press, April 26, 2010, DOI 10.1074/jbc.M110.106849

Cecilia Brännmark^{‡1}, Robert Palmér[‡], S. Torkel Glad[§], Gunnar Cedersund^{‡¶1,2}, and Peter Strålfors^{‡3}

From the [‡]Division of Cell Biology, Department of Clinical and Experimental Medicine, Laboratory of Diabetes and Integrated Systems Biology, and the [§]Department of Electrical Engineering, Linköping University, SE58185 Linköping, Sweden and the

[¶]Freiburg Institute for Advanced Studies, School of Life Sciences, Albert-Ludwigs-Universität Freiburg, D79104 Freiburg, Germany

Insulin and other hormones control target cells through a network of signal-mediating molecules. Such networks are extremely complex due to multiple feedback loops in combination with redundancy, shared signal mediators, and cross-talk between signal pathways. We present a novel framework that integrates experimental work and mathematical modeling to quantitatively characterize the role and relation between co-existing submechanisms in complex signaling networks. The approach is independent of knowing or uniquely estimating model parameters because it only relies on (i) rejections and (ii) core predictions (uniquely identified properties in unidentifiable models). The power of our approach is demonstrated through numerous iterations between experiments, model-based data analyses, and theoretical predictions to characterize the relative role of co-existing feedbacks governing insulin signaling. We examined phosphorylation of the insulin receptor and insulin receptor substrate-1 and endocytosis of the receptor in response to various different experimental perturbations in primary human adipocytes. The analysis revealed that receptor endocytosis is necessary for two identified feedback mechanisms involving mass and information transfer, respectively. Experimental findings indicate that interfering with the feedback may substantially increase overall signaling strength, suggesting novel therapeutic targets for insulin resistance and type 2 diabetes. Because the central observations are present in other signaling networks, our results may indicate a general mechanism in hormonal control.

Hormonal control of target cells involves signal transduction from ligand-activated receptors to control of rate-limiting enzymes or proteins that affect key steps in metabolism or other processes within the cell. The signal transduction is carried out by a network of interacting signal mediators. A high degree of

complexity is due to the presence of feedback and feed-forward loops, both negative and positive, and the fact that the importance of different interactions changes over time and according to intracellular location. This, in combination with redundancy, shared signal mediators, shared signal paths, and ample cross-talk between signals, leads to a complexity that poses new challenges to progress in dissecting and understanding cellular control. Many diseases, such as cancer and insulin resistance and type 2 diabetes, arise from malfunctioning in signaling networks.

Insulin controls target cells through binding to its receptor at the cell surface (1), which activates the intracellular domains of the insulin receptor (IR)⁴ to trans-autophosphorylate at specific tyrosine residues. The receptor can then transduce the insulin signal into the cell and to its various effectuating systems, such as glucose uptake and antilipolysis. Foremost of the directly downstream signal-mediating proteins are members of the insulin receptor substrate (IRS) family, in particular IRS1, which is rapidly phosphorylated at specific tyrosine residues by the activated receptor. The IR and IRS1 are in adipocytes colocalized to caveolae invaginations of the plasma membrane (2–5). IR is rapidly endocytosed in response to insulin stimulation of adipocytes, and it appears that the phosphorylated receptor is internalized into the endosomal compartment (6, 7). In accordance with the known properties of caveolae, very little IR is internalized in the absence of insulin stimulation (6). The function of internalization is not clear, and suggestions implying both positive and negative effects have been proposed: down-regulation of the insulin response by receptor degradation, clearance of insulin from the circulation by insulin digestion, and internalization as part of the insulin signal transduction.

Insulin signaling and the role of internalization illustrate a general limitation in our understanding of signaling systems; the central skeleton has often been established, but the quantitative importance of states and subprocesses remains undetermined. For instance, although a signaling intermediate (a specific state of a protein or a protein complex) has been established as mediating the signal transduction, it is typically not known how quickly it is formed and eliminated or how its absolute concentration varies over time. It is also

* This work was supported by the European Commission Network of Excellence Biosim, Östergötland County Council, Novo Nordisk Foundation, Lions, Swedish Diabetes Association, and Swedish Research Council.

[5] The on-line version of this article (available at <http://www.jbc.org>) contains supplemental Figs. S1–S3 and Methods.

¹ Both authors contributed equally to the work.

² To whom correspondence may be addressed: Dept. of Clinical and Experimental Medicine, Linköping University, SE58185 Linköping, Sweden. Tel.: 46-702-512323; Fax: 46-13-224149; E-mail: gunnar.cedersund@liu.se.

³ To whom correspondence may be addressed: Dept. of Clinical and Experimental Medicine, Linköping University, SE58185 Linköping, Sweden. Tel.: 46-13-224315; Fax: 46-13-224149; E-mail: peter.stralfors@liu.se.

⁴ The abbreviations used are: IR, insulin receptor; IRS1, insulin receptor substrate-1; ODE, ordinary differential equation.

Integrated Experimental/Modeling Analysis

typically not known how important a particular state or sub-process is for the overall signal transduction process. These limitations have remained because, except in special cases, we can neither measure nor perturb such detailed states and subprocesses individually but only indirectly through perturbations and measurements of lumped states. The processes are also so intertwined that conclusions about the details of the processes cannot be obtained by biochemical reasoning. Mathematical modeling emerges as a potent tool for data analysis and for dissection of such complex processes. However, the study of biological signaling systems poses new challenges also for mathematical modeling. The complexity of the underlying processes implies that the hypotheses the mathematical models seek to capture involve many parameters, whose values typically depend on cell type, experimental conditions, etc. For this reason, the individual parameter values usually remain underdetermined (*i.e.* guessed or non-uniquely estimated). This is an important problem because, if not accounted for, it implies that also the conclusions and predictions from the model will be non-unique and sometimes even arbitrarily unreliable.

We here report a comprehensive integrated experimental/mathematical modeling study that presents a framework to circumvent the problem of undetermined parameter values. We used numerous iterations between experiments, model-based data analysis, and theoretical predictions to characterize the early phase of insulin signaling in primary human adipocytes. We show that an internalization-mediated feedback mechanism is a necessary component in producing an observed signal overshoot. These new mechanistic insights demonstrate that an integrated mathematical-experimental approach is a powerful analysis tool, which has the potential to overcome some of the hurdles to progress posed by the inherent complexity of signaling networks.

MATERIALS AND METHODS

Subjects—Abdominal subcutaneous fat was obtained from elective abdominal surgery at the University Hospital in Linköping. Informed consent was obtained from participating individuals; procedures were approved by the local ethics committee at Linköping University and were performed in accordance with the Declaration of Helsinki.

Materials—Mouse anti-phosphotyrosine (PY20) monoclonal antibodies were from Transduction Laboratories (Lexington, KY). Rabbit anti-IRS1 polyclonal and mouse anti-phosphotyrosine (4G10) monoclonal antibodies were from Upstate Biotechnology, Inc. (Lake Placid, NY). Rabbit polyclonal anti-insulin receptor β -subunit and anti-actin antibodies were from Santa Cruz Biotechnology, Inc. (Santa Cruz, CA). Methyl- β -cyclodextrin was obtained from Sigma.

Isolation and Incubation of Adipocytes—Adipocytes were isolated from subcutaneous adipose tissue by collagenase (type 1; Worthington) digestion as described (8). Cells were treated and incubated in supplemented Krebs-Ringer solution as described (9).

SDS-PAGE and Immunoblotting—To minimize postincubation signaling and protein modifications, which can occur during immunoprecipitation, cells were immediately dissolved in

SDS and β -mercaptoethanol with protease and protein phosphatase inhibitors, frozen within 10 s, and thawed in boiling water for SDS-PAGE and immunoblotting (8). Membranes were incubated with antibodies and detected using ECL+ (Amersham Biosciences) with horseradish peroxidase-conjugated anti-IgG as secondary antibody, evaluated by chemiluminescence imaging (Las 1000, Fuji, Tokyo, Japan), and normalized against the amount of actin in each sample.

Determination of IR Internalization—An intracellular membrane fraction of adipocytes, preincubated with or without 100 nM insulin for 10 min, was prepared by homogenization as described (10). The homogenate was centrifuged at $1000 \times g$ for 10 min to remove fat, nuclei, and cell debris. Plasma membrane and mitochondria were removed by centrifugation of the $1000 \times g$ supernatant at $16,000 \times g$ for 20 min. The supernatant was centrifuged at $210,000 \times g$ for 75 min to pellet intracellular membranes. The pellet was resuspended in 50 mM Tris, pH 7.4, with 1 mM EDTA and a mixture of protease inhibitors. Control and insulin-stimulated whole cell lysates and the intracellular membrane fractions were compared using SDS-PAGE and immunoblotting for the IR.

Mathematical Models—Models are formulated using ordinary differential equations (ODEs) with the following notation,

$$dx/dt = f(x,p) \quad (\text{Eq. 1})$$

$$y = g(x,p) \quad (\text{Eq. 2})$$

where x represents the states (here corresponding to concentrations or amounts of the specific protein modifications); p represents kinetic constants or scaling parameters; y contains the measurement signals; and f and g are smooth well behaved nonlinear functions. All models analyzed in this work are presented as interaction graphs in [supplemental Fig. S1](#). These interaction graphs exactly describe the dynamic part of the ODE (the function $f(x,p)$), if the reaction rates are given, according to the standard summation of rates, which is briefly summarized in Ref. 12 and in the [supplemental material](#). The reaction rates are described by mass action kinetics, possibly modified by multiplication with the concentration of the protein kinase. The output function, $g(x,p)$, corresponds to normalizations and unknown scaling factors between the concentrations or amounts and the measured signals. These normalizations and optimizations are fully described along with all used Matlab scripts in the [supplemental material](#).

All models are denoted M followed by an italic letter specifying the corresponding hypothesis (d, m, f, i , or if). A final letter (a, b, c, or d) specifies the specific model structure, which becomes a model if the model structure is associated with a set of parameter values.

A Modified Optimization Approach—A key aspect of our approach is that it is not centered around specific parameter values that need to be known or estimated, but around data and model structures, which implicitly determine the entire set of acceptable parameters. The characterization of this set requires non-standard optimization algorithms, which do not return a single (ideally global) optimum but return sets of parameters giving a cost lower than a certain threshold. We are then look-

ing for model properties that are shared among all of these parameter values. The optimization algorithms should therefore ideally return widely spread acceptable parameters. Because no such optimization algorithms are readily available, we modified a simulated annealing approach, which was implemented in the Systems Biology Toolbox for MATLAB, to fit our purposes. This annealing approach is normally combined with a nonlinear simplex, which is searching locally and downhill for low temperatures, but potentially also uphill for higher temperatures. Here the term “temperature” describes how much the search algorithm may proceed to parameters with higher cost function values. The temperature is lowered in discrete steps, and for each new temperature in the standard implementation, a single new simplex is initiated at the best parameter found so far. The key modification in our modified algorithm is to restart several new simplexes, which lie far away from each other according to a certain distance measure. This distance measure is basically the Euclidian distance, using a standard modification that takes the dimensionality of the optimization problem into account. Then all parameters evaluated during the optimization and with a cost below the given threshold are saved and analyzed using simulations and manual inspections. We are particularly interested in model properties that are shared among all acceptable parameter sets, which we denote core predictions. Previous analysis on test problems with analytically known cost functions showed that this new algorithm appears to be a robust and well functioning approach for the 5–25 dimensional problems that we encounter (11).⁵ Note that this approach gives an improved spread of the parameters without modifying the cost function. More technical details concerning the optimization and the new algorithm are given in the [supplemental material](#), and the implemented algorithm is provided along with the optimization scripts. The entire approach is outlined in Fig. 3 and is further described under “Results and Discussion.”

Statistical Analysis and Assumptions—The core prediction analysis is used to identify experiments that (if the core predictions are not fulfilled) should reject the model, but the actual rejection is done using classical optimization and hypothesis testing methods. Once a core prediction has been measured experimentally, the model giving the prediction is optimized to the expanded data set, and tested using a χ^2 test (13).

Our choices for the modeling were based on a number of assumptions. We used ODEs because we do not have data with a high spatial resolution, and the natural assumption is to consider the cells as well mixed. Further, we modeled the internalization of IR and IRS1 as independent processes and restricted the possibilities for insulin binding and dissociation to avoid combinatorial explosion. We assumed that the noise can be approximated by purely measurement noise, that it is normally distributed, and that the S.E. value can be approximated by repeats of the same experiment.

RESULTS AND DISCUSSION

Hypotheses and Mechanistic Models for Early Insulin Signaling—To better understand the role of internalization and other mechanisms that govern the initial phase of insulin signaling, we (12) examined the phosphorylation of IR and IRS1 in

human primary adipocytes. We found a transient overshoot in the steady-state phosphorylation of both IR and IRS1; the phosphorylation reached a peak within 2 min of the addition of insulin, followed by a lower quasi-steady-state phosphorylation (Fig. 1, A–C). In Ref. 12, we analyzed what conclusions can be drawn from this overshoot observation alone. That the overshoot appeared already in the phosphorylation of the IR implies that we should look for mechanisms that negatively affect the phosphorylation of IR directly but with a time delay. In Ref. 12, we rejected a large number of model structures and identified two fundamentally different acceptable model structures, which could not be rejected or distinguished from those data. In this work, we further characterize the system using an iterative experimental/theoretical modeling approach. We start by introducing two new non-rejectable hypotheses, giving a total of four fundamentally different mechanisms that can generate the observed overshoot (Fig. 2): (i) insulin degradation (*i.e.* decreased phosphorylation because the concentration of insulin in the medium is being reduced (*Md*)); (ii) competitive inhibition and other interaction schemes at the plasma membrane alone (*Mm*); (iii) negative feedback signals from downstream intermediates (*Mf*); (iv) down-regulation through internalization and dephosphorylation of IR (*Mi*).

These hypotheses are negative feedbacks but of a fundamentally different character: some (*e.g.* iv) involve transfer of molecules, and some (*e.g.* iii) involve transfer of information. They include the assumption that non-stated mechanisms are not present in such a way that they might cause the overshoot. For instance, the degradation hypothesis might include internalization but not the crucial dephosphorylated internalized state that leads to an overshoot from the internalization itself (12) ([supplemental Fig. S1](#)). We examine various detailed variations of these hypotheses, and details are added only as they are needed to explain additional experimental data sets (all models and Matlab scripts are available as downloadable simulation and optimization files; see “Materials and Methods”). The different versions of a hypothesis are implemented through different model structures and referred to as, for example, *Mda* or *Mdb*, which correspond to the first and second version of the degradation hypothesis, etc. (see “Materials and Methods”).

Rejection of the Insulin Degradation Model through Statistical Testing and through Experimental Testing of Uniquely Identified Core Predictions—In hypothesis *Md*, insulin is degraded so that the concentration of insulin is declining in the medium (*e.g.* by insulin binding to IR followed by lysosomal degradation or by insulin-degrading enzymes at the cell surface) (Fig. 2). This hypothesis can indeed produce an overshoot behavior (Fig. 1, B and C). We will now show why this hypothesis is rejected anyway and in the process introduce the two main steps of our analysis: (i) hypothesis testing based on experimental data and (ii) experimental testing of uniquely identified core predictions (Fig. 3).

The first *Md* model we tested, *Mda* ([supplemental Fig. S1](#)), includes only insulin degradation through lysosomal degradation. *Mda* includes internalization, but it does not include the crucial state that has been dephosphorylated but not yet recycled to the plasma membrane. This model structure does not produce an overshoot due to the internalization itself (*i.e.* if

⁵ G. Cedersund, manuscript in preparation.

Integrated Experimental/Modeling Analysis

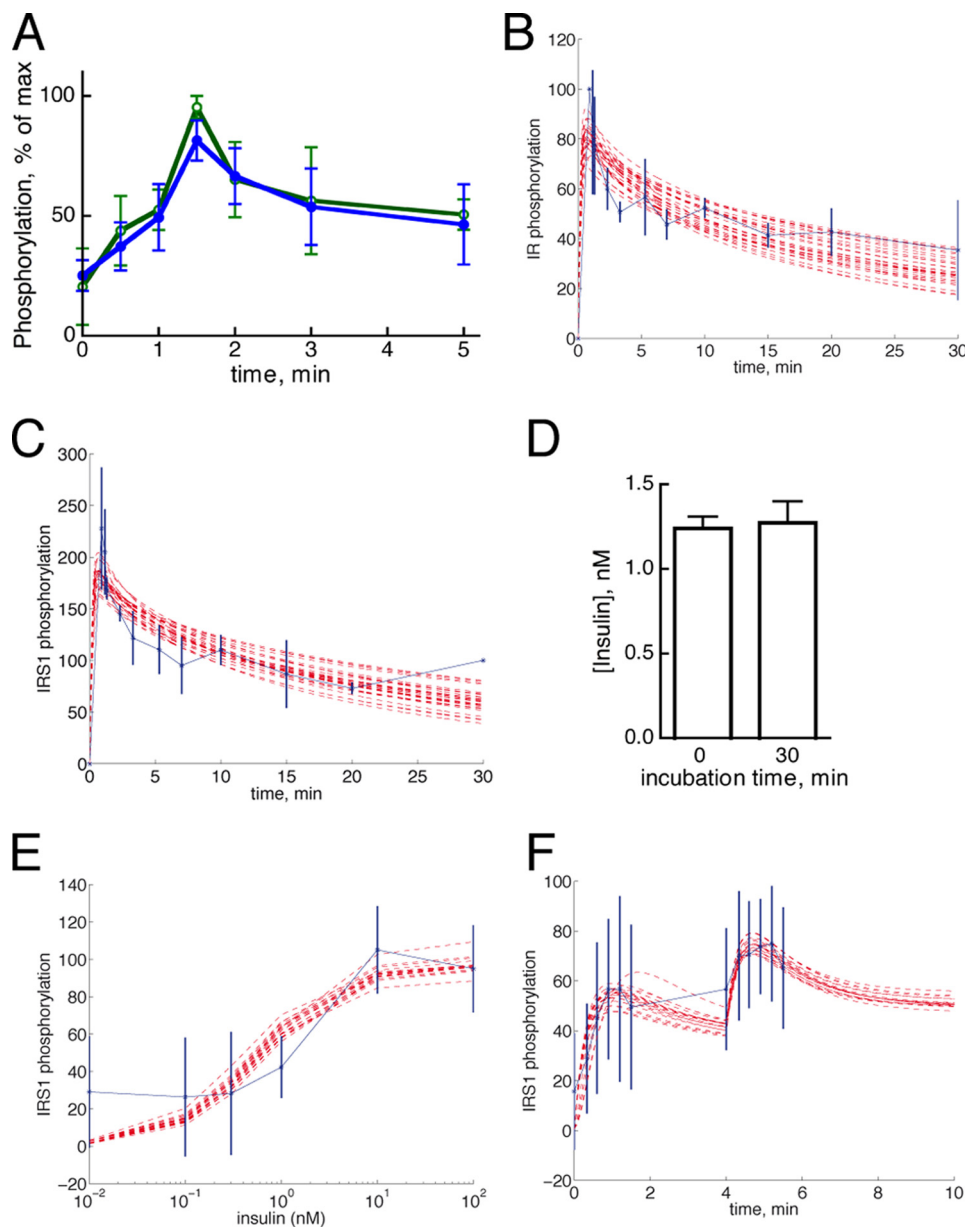


FIGURE 1. Experimental data and core predictions for overshoot behavior. *A*, short term detailed time course for phosphorylation of IR (green) and IRS1 (blue) in response to 10 nM insulin. The extent of phosphorylation is expressed as a percentage of maximum in each experiment ($n = 4$ (IR) and $n = 5$ (IRS1), independent experiments, subjects) and presented as mean \pm S.E. (error bars). *B*, the experimental data for phosphorylation of IR in response to 100 nM insulin (mean \pm S.D. (error bars), blue) are compared with different simulations that correspond to acceptable parameters for model *Mdd* (red). *C*, the experimental data for phosphorylation of IRS1 in response to 100 nM insulin (mean \pm S.D. (error bars), blue) are compared with different simulations that correspond to acceptable parameters for model *Mdd* (red). *D*, experimental determination of insulin concentration. Adipocytes were incubated with insulin for 30 min. The concentration of insulin in the medium was determined directly after the addition of insulin and after 30 min. Insulin was determined by enzyme-linked immunosorbent assay, using a kit from Merckodia (Uppsala, Sweden). Values are mean \pm S.E. (error bars), $n = 3$. *E*, steady-state dose-response phosphorylation of IRS1 in response to the indicated concentration of insulin after a 10-min incubation. The extent of phosphorylation is expressed as a percentage of maximum (mean \pm S.D. (error bars)) ($n = 7$, independent experiments, subjects) (blue) and compared with different simulations that correspond to acceptable parameters for model *Mmb* (red). *F*, time course for phosphorylation of IRS1 in response to a two-step addition of insulin to a final concentration of 1.2 nM at 0 min and 10 nM at 4 min. The extent of phosphorylation is expressed as a percentage of maximum (mean \pm S.D. (error bars)) ($n = 8$, independent experiments, subjects) (blue) and compared with different simulations that correspond to acceptable parameters for model *Mmb* (red).

insulin is a fixed parameter) (12). However, when insulin is considered as a limited pool in an extracellular volume reasonably different from the intracellular volume, the model can produce an overshoot (supplemental Fig. S2, A and B). This model

structure is accepted, and we proceed to phase II, core prediction analysis.

Despite different ways and widely different parameters for producing the overshoot with this model structure, all of them exhibit the peak of IR phosphorylation (but not of IRS1 phosphorylation) earlier than 0.1 min (supplemental Fig. S2A and Table 1). We refer to that type of uniquely identified properties as core predictions. This concept, which has been introduced by us (13), relieves us from the limitation of interpreting results for one particular set of parameter values. The problem with analysis at a single parameter point is that parameter values usually are more or less guessed or non-uniquely estimated from the experimental data; this leads to similarly guessed or non-uniquely estimated model predictions. In practice, we identify the uniquely identified core predictions by first approximating the entire space of acceptable parameters (*i.e.* all parameters that yield cost functions that are statistically indistinguishable from the best value). Importantly, our optimization method is designed to especially search for acceptable parameters that lie far away from each other in a Euclidian fashion without adding an extra modification to the cost function (see “Materials and Methods” and supplemental material). We then analyze the model behavior over this entire set of parameters, and model properties that are shared among all acceptable parameters are considered as core predictions (Fig. 3).

Mda thus has the core prediction that the time of the peak phosphorylation of IR occurs before 0.1 min. Experimentally, a lower boundary for the time of the peak value of IR phosphorylation was around 1 min (Fig. 1A). Hence, the core prediction of *Mda* is not fulfilled, and the model should probably be rejected.

We also tested two other similar model structures, *Mdb* and *Mdc* (supplemental Fig. S1). These are more complex variations of *Mda* but differ only in that they have more internalized states and more reactions between the states. Nevertheless, also these model structures are unable to

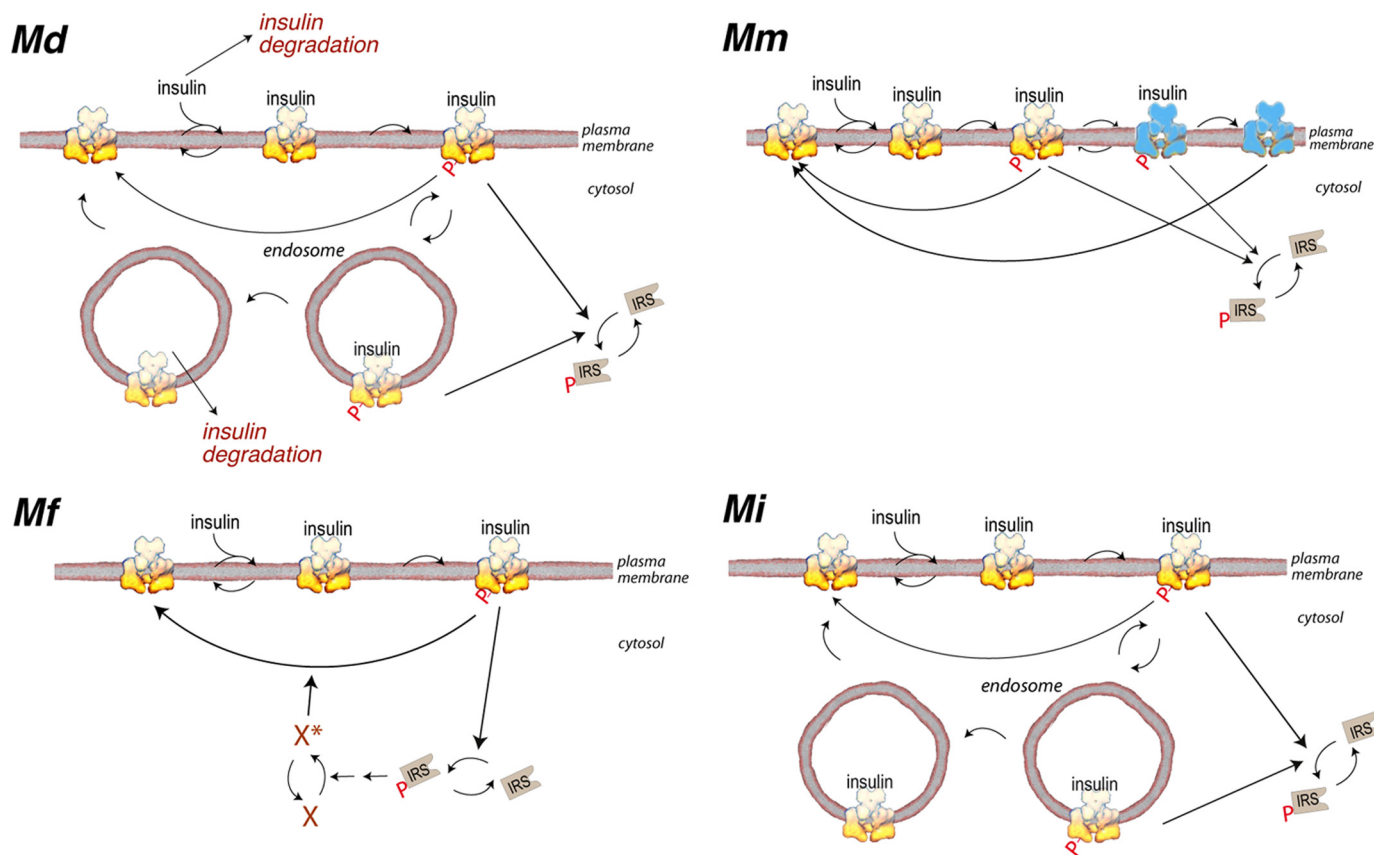


FIGURE 2. **Outlines of the four main hypotheses for explanation of overshoot behavior.** Shown are insulin degradation (*Md*), complicated interactions at the plasma membrane (*Mm*), feedbacks from downstream intermediates (*Mf*), and internalization of IR (*Mi*).

produce a peak value for IR phosphorylation later than 0.1 min and should thus probably also be rejected.

To validate the predicted rejections, we undertook a more conventional two-step hypothesis testing approach. First, the models were optimized to the complete data set, here including both the overshoot data (Fig. 1, *B* and *C*) and the experimentally measured peak time (1.3 ± 0.2 min). Note that this involves a classical optimization, seeking only the best parameters, and that the cost function should be a χ^2 measure without *ad hoc* punishments. Second, the resulting agreement with the data is evaluated using a χ^2 test. For the most complex model, *Mdc*, this gave a test function value of 116, which should be compared with a threshold of 38.9 for a 95% χ^2 distribution with 26 degrees of freedom (the number of data points). In other words, the core prediction successfully identified a crucial experiment (*i.e.* an experiment that implies a rejection of the model if the core prediction is not fulfilled); this serves as a validation of the core prediction analysis.

We identified one model structure that does not have the problem of a too early peak time: *Mdd* (supplemental Fig. S1). This model structure includes insulin degradation both through lysosomal degradation and through direct degradation in the extracellular medium (corresponding to insulin-degrading processes at the plasma membrane). *Mdd* does not have the same spike-like rise in IR phosphorylation (Fig. 1*B*) and is able to produce a rise that is equally smooth as that produced by *Mda* to *-c* for phosphorylation of IRS1 only (Fig. 1*C*). We therefore looked for core predictions also for *Mdd* and found one that

could be experimentally tested, the extracellular concentration of insulin. *Mdd* predicts that >95% of the insulin is degraded within the first few min (supplemental Fig. S2*D*). This prediction is shared among all acceptable parameter values and is thus a core prediction (*i.e.* a uniquely identified model property). Experimentally, the extent of degradation of insulin over 30 min was negligible (Fig. 1*D*). The core prediction is thus not fulfilled, and also *Mdd* should probably be rejected. We validated this core prediction-based rejection in the same way as above, by fitting the model to the complete data set (overshoot and amount of degradation) and evaluating the agreement using a χ^2 test. The test function gave a value of 80, which should be compared with a χ^2 threshold value of 38, implying a validated rejection. All of this evidence taken together led us to reject the *Md* hypothesis (see Table 2, which summarizes this and all similar conclusions).

Collection of a Set of Standard Data; Single-step, Double-step, and Dose-response Curves—To differentiate between the three remaining acceptable explanations for the overshoot data (*Mm*, *Mf*, and *Mi*) (Fig. 2), we searched to find experimentally testable core predictions that are different in these different hypotheses. However, the uncertainty of the predictions was too high (supplemental Fig. S2, *N* and *O*). Furthermore, many of the predicted behaviors lay outside the known behaviors of the system. For instance, the remaining models could at this point predict that 100 nM insulin treatment corresponds to less than 10% of maximal response (supplemental Fig. S2*N*), whereas we know that 100 nM treatment corresponds to saturation and

Integrated Experimental/Modeling Analysis

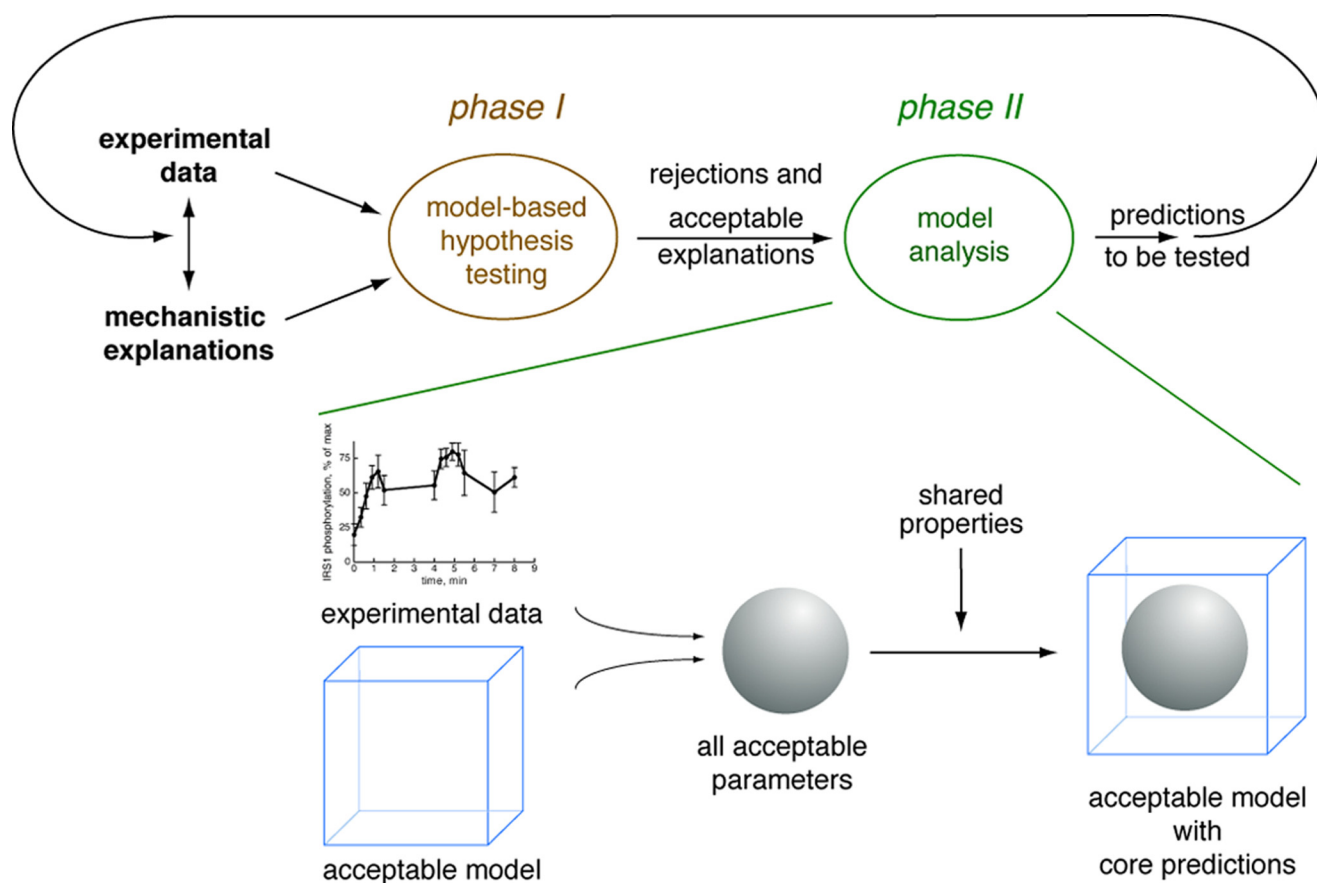


FIGURE 3. **Outline of the experimental/modeling strategy.** The upper part shows the two main steps (phases I and II) in the modeling that can be done robustly for unidentifiable models. The lower part shows phase II in more detail: calculations of core predictions (*i.e.* uniquely identified model properties also for unidentifiable models).

TABLE 1
Spread of parameters for model *Mdc*

Columns 2 and 3 show the maximum and minimum values found by our modified optimization algorithm (*i.e.* when searching for all acceptable parameters giving a non-rejectable agreement with the overshoot data). As can be seen, many parameters can take values over many orders of magnitude. The last two columns display the boundaries set for the search. Note that some found values lie slightly outside these boundaries because the optimization algorithm sometimes evaluates such points as well. All parameters, models, and optimization scripts for all evaluated models are available in the [supplemental material](#).

Parameter name	Maximum found	Minimum found	Maximum boundary	Minimum boundary
k_1	59	0.38	5e5	1e-5
k_{m1}	7.3e4	1e-5	5e5	1e-5
k_2	6.2e5	6.2e2	5e5	1e-5
k_3	3.6e5	4.9e3	5e5	1e-5
k_{m3}	76	1e-5	5e5	1e-5
k_4	5.8e5	1e-5	5e5	1e-5
k_5	5e5	1.8e3	5e5	1e-5
k_6	7	0.21	5e5	1e-1
k_{m6}	11	2.2	15e4	1e-1
k_{y1}	5.3e3	46	1e5	10
k_{y2}	4.4e3	10	1e5	10
k_{y3}	5.9e3	45	1e5	10
k_{y4}	3.5e3	10	1e5	10
Volfrac	0.013	0.001	0.01	0.001
k_7	6.2e5	0	5e5	0

maximal response. To avoid these problems with realism and nonspecific predictions, we collected more informative data: dose responses and multiple stimulations with insulin (Fig. 1, *E* and *F*). We refer to the resulting data (Fig. 1, *B*, *C*, *E*, and *F*) as the standard data. The three hypotheses *Mm*, *Mf*, and *Mi* are all able to describe these standard data ([supplemental Figs.](#)

TABLE 2
Summary of the data, models, and conclusions

Rows correspond to different sets of data, and columns correspond to different hypotheses. OK indicates that the hypothesis can explain the data, and Fail indicates that the hypothesis is rejected.

Experimental data	Models				
	<i>Md</i>	<i>Mm</i>	<i>Mf</i>	<i>Mi</i>	<i>Mfi</i>
Overshoot	OK	OK	OK	OK	OK
Insulin in medium	Fail	OK	OK	OK	OK
Standard data		OK	OK	OK	OK
Blocking of internalization		Fail	Fail	OK	OK
Extent of internalization				Fail	OK

S2 (I-M) and *S3 (D-G)*, although some specific model structures could be rejected: *Mma*, *Mia*, and *Mfa* ([supplemental Figs. S1, S2H, and S3C](#)). Further, previously identified uncertain or unrealistic predictions are now much improved (compare [supplemental Fig. S2O](#) with [supplemental Fig. S2P](#)).

Testing of Different Core Predictions with Respect to Blocking of Internalization—We now return to identification of core predictions that can distinguish between the remaining hypotheses. Blocking of internalization is an experiment where the three hypotheses yield different predictions; *Mf* and *Mm* predict that the overshoot remains, but *Mi* predicts that it disappears ([supplemental Fig. S3I](#)).

We blocked endocytosis of IR by lowering the temperature, which eliminates membrane vesicularization and fission (14). At 11 °C, the transient phosphorylation overshoot was gone

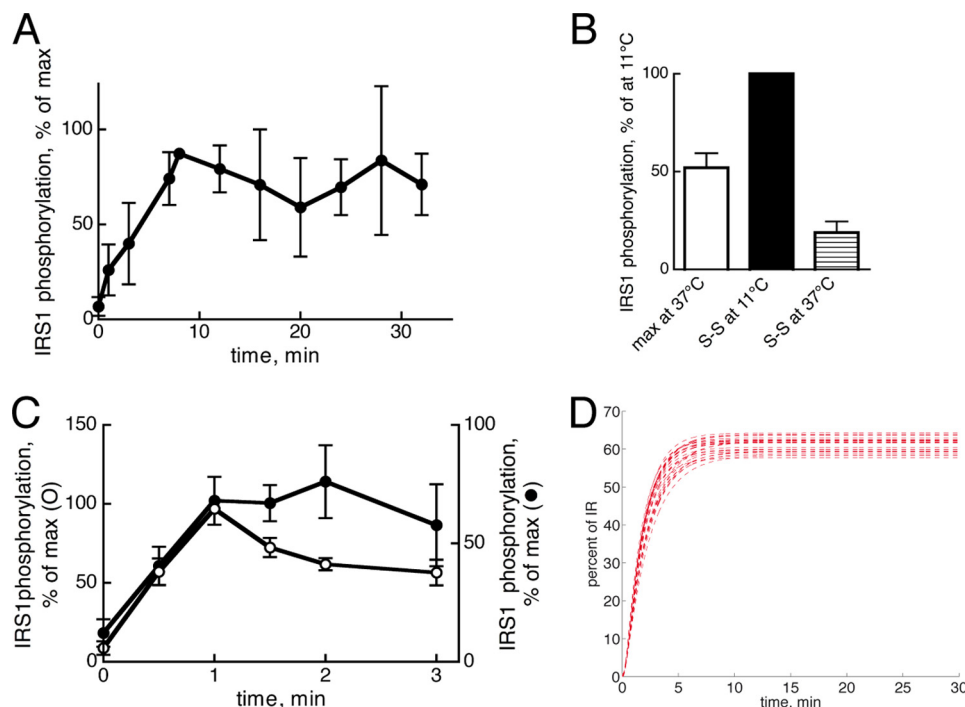


FIGURE 4. Analysis of the importance of IR internalization for generation of overshoot behavior. *A*, time course for phosphorylation of IRS1 in response to 10 nM insulin at 11 °C. The extent of phosphorylation is expressed as a percentage of maximum in each experiment and presented as mean \pm S.E. (error bars) ($n = 3$, independent experiments, subjects). *B*, comparison of maximum and steady-state phosphorylation of IRS1 at 11 and 37 °C. The extent of phosphorylation is expressed as a percentage of steady state at 11 °C, mean \pm S.E. (error bars) ($n = 5$, independent experiments, subjects). *C*, time course for phosphorylation of IRS1 in response to 10 nM insulin with (filled symbols) or without (open symbols) preincubation of cells with 8 mM methyl- β -cyclodextrin for 50 min. The extent of phosphorylation is expressed as a percentage of maximum in each experiment and presented as mean \pm S.E. (error bars) ($n = 6$, independent experiments, subjects). *D*, core predictions for the model *Mic* regarding requirement for internalization of IR, expressed as a percentage of IR that has to be internalized and dephosphorylated at different times after the addition of insulin.

(Fig. 4A). Lowering the temperature also reduced the response time because a lower temperature implies smaller rate constants. Interestingly, both the maximal and steady-state phosphorylation levels in response to insulin were increased (Fig. 4B). This shows that interfering with the mechanisms causing the overshoot may significantly increase the signaling strength. Because cooling is a rather nonspecific intervention, we also blocked internalization by reducing the amount of cholesterol in the plasma membrane, which eliminates caveolae invaginations in fat cells (15) and therefore IR internalization (6). Also, this inhibition of IR internalization removed the overshoot (Fig. 4C) with a significance of <0.05 (see “Materials and Methods”), which also implies a significant rejection of hypotheses *Mm* and *Mf* (Table 2).

Internalization Is Not a Sufficient Mechanism—In a final iteration of the analysis experiment cycle (Fig. 3), we now show that the remaining hypothesis *Mi* has to be rejected as well. We have showed that the internalization model *Mi* has to include the state *IRi*, which is internalized and dephosphorylated but not yet recycled to the plasma membrane and available to be phosphorylated (12). A core prediction analysis showed that within a few min this state must account for 55–80% of the total amount of receptors (Fig. 4D). Hence, more than 55% of IR should be found in the internalized, cytosolic compartment after insulin stimulation. We experimentally determined the fraction of IR that was internalized after stimulation with insulin and found

that only $2.3 \pm 0.8\%$ (mean \pm S.E., $n = 3$ independent experiments, subjects) of the total amount of receptors was recovered in the intracellular compartment. This argues that model *Mi* should be rejected.

We again validated this core prediction-based rejection using a classical hypothesis testing approach; we fitted the model to the complete data set (standard data plus the amount of internalization) and found a test function value of 221, which is way beyond the threshold 61, corresponding to the 95% χ^2 value for 44 degrees of freedom.

This rejection depends on our ability to search the space of acceptable parameters, and to further examine also this assumption leading to the rejection, we did some additional analytical analysis. We showed that decreasing a parameter at some point in a circular and mildly nonlinear model structure (such as *Mma*) eventually leads to overshoots in the preceding states (supplemental material, Corollary 1). This is also accompanied by an increase in the steady-state concentration of the following state (such

as *IRi* in *Mia-c*). We give analytical expressions for these dependences (e.g. supplemental Equation 11). Hence, both an overshoot and an increased steady state are caused by the same changes. These results underscore our numerically derived insights and, together with our experimental data, lead to rejection of hypothesis *Mi*.

The Final Acceptable Model, with an Internalization-dependent Negative Feedback—All initially proposed hypotheses have now been rejected (Table 2). The rejection of *Mi* showed that it is not the internalization *per se* that generates the overshoot. We therefore examined a combination of *Mf* and *Mi*, *Mif*, where the feedback in *Mf* is dependent on internalization (Fig. 5A). This model can explain all available data for early insulin signaling (Fig. 5, B–G), it passes a χ^2 test, and it is thus our final model for the system. Note that the model includes feedbacks from mass (internalization and recycling) and information transfer (through signaling via intermediary *X*) and that both of those feedbacks are required.

The model requires that only a small fraction of IR is internalized at steady state but also that internalization is essential for the signaling. A core prediction analysis of the model reveals that internalized receptors are not significantly stronger signal generators than those at the plasma membrane (i.e. the catalyzing parameters for the two pools of autophosphorylated receptors are of the same order of magnitude). Instead, the requirement for the small, internalized pool is due

Integrated Experimental/Modeling Analysis

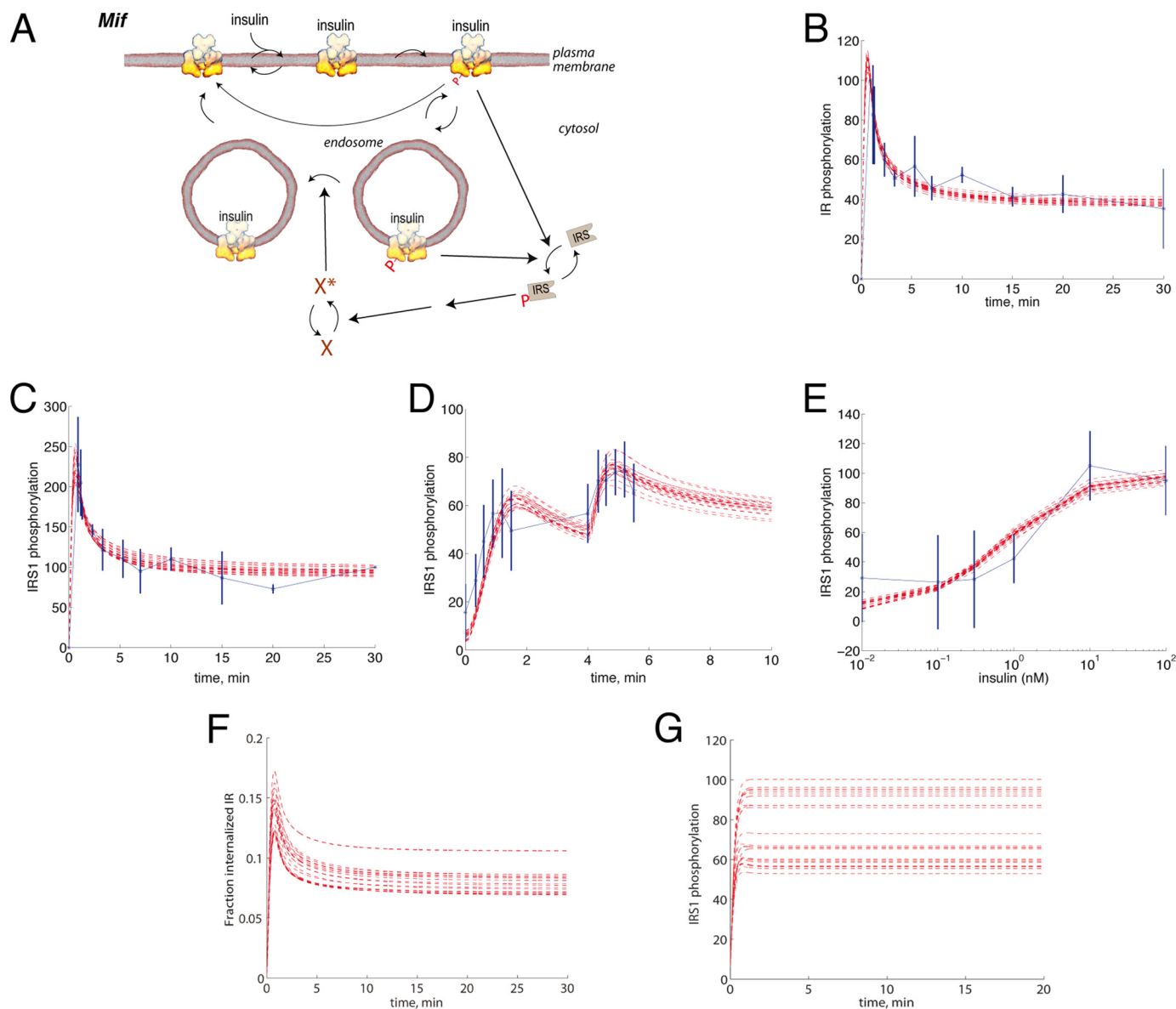


FIGURE 5. Results from simulation with the final model structure, hypothesis *Mif* (in red), compared with experimental data (in blue). *A*, outline of the final hypothesis *Mif*. *B*, time course for IR phosphorylation in response to 100 nM insulin (mean \pm S.D. (error bars)). *C*, time course for IRS1 phosphorylation in response to 100 nM insulin (mean \pm S.D. (error bars)). *D*, time course for phosphorylation of IRS1 in response to a two-step addition of insulin to 1.2 nM at 0 min and 10 nM at 4 min (mean \pm 0.5 S.D. (error bars)). *E*, steady-state dose-response phosphorylation of IRS1 in response to the indicated concentration of insulin after a 10-min incubation (mean \pm S.D. (error bars)). *F*, simulations of the amount of IR in the internalized, dephosphorylated state. *G*, simulations of the behavior of IRS1 phosphorylation when internalization is blocked.

to rapid internalization of the autophosphorylated IR, such that there is more phosphorylated IR in the internalized pool, compared with at the plasma membrane. This prediction is consistent with experimental results (6, 7). Signal overshoot behavior is found in responses to other hormones and in other cell types (e.g. in response to isoprenaline in adipocytes (8), epidermal growth factor in epithelial cells (16), and Hedgehog in *Drosophila* (17)). Our findings may therefore indicate a general mechanism not restricted to insulin signaling.

We want to stress some not yet mentioned general insights regarding the modeling framework we have developed. First, it results in an analysis including unique predictions and rejections rather than just a final mathematical model. Second, our approach to analysis, and hence our final model, is only concerned with mechanisms that are essential to the observed

dynamics and is not attempting to generate a complete description of all processes that are involved. Our analysis goes beyond such descriptive usages of modeling. Third, our parameter-free conclusions are strong and final in that they will not be revised in the future; a rejected model may never describe a larger data set, and a uniquely identified property may not become non-unique from more data. This strength and finality do not exist with ordinary usage of models, including in some of the previous modeling works on insulin signaling (18–21) and insulin binding (21–24). Fourth, note that all conclusions drawn in the paper are independent of the theoretical underpinnings of our core prediction analysis and modified optimization algorithm. Nevertheless, because all core prediction-based rejections were successfully validated, our work may in itself indicate the existence of such a theoretical underpinning. Fifth, we generally do

not make claims regarding untested models, parameters, or combinations of mechanisms. For instance, we almost exclusively deal with mass action kinetics, and there might exist models with more complicated rate expressions that would give a different core prediction for the same interaction graph. There might also exist combinations of mechanisms other than our *Mif* hypothesis that also give acceptable behaviors with respect to the final data set. Nevertheless, any combination of mechanisms that does not include internalization of IR cannot explain the data because experimental blocking of the internalization showed that the overshoot then disappears. This thus allows us to refer to internalization as “necessary.” Note that this specific conclusion depends on the assumption that the two types of experimental blockings (cooling and removal of cholesterol) are specific, which is the typical limitation of purely experimental studies. Note also that our modeling approach can complement this weakness by adding stronger statements, of the character “not sufficient.”

In summary, we have thus concluded that receptor internalization is necessary but not sufficient for control of insulin signaling and that the internalization mediates at least two fundamentally different types of feedbacks: via mass-transport and via information transfer.

REFERENCES

1. Taniguchi, C. M., Emanuelli, B., and Kahn, C. R. (2006) *Nat. Rev. Mol. Cell Biol.* **7**, 85–96
2. Gustavsson, J., Parpal, S., Karlsson, M., Ramsing, C., Thorn, H., Borg, M., Lindroth, M., Peterson, K. H., Magnusson, K. E., and Strålfors, P. (1999) *FASEB J.* **13**, 1961–1971
3. Karlsson, M., Thorn, H., Danielsson, A., Stenkula, K. G., Ost, A., Gustavsson, J., Nystrom, F. H., and Strålfors, P. (2004) *Eur. J. Biochem.* **271**, 2471–2479
4. Foti, M., Porcheron, G., Fournier, M., Maeder, C., and Carpentier, J. L. (2007) *Proc. Natl. Acad. Sci. U.S.A.* **104**, 1242–1247
5. Stenkula, K. G., Thorn, H., Franck, N., Hallin, E., Sauma, L., Nystrom, F. H., and Strålfors, P. (2007) *Biochem. Biophys. Res. Commun.* **363**, 840–845
6. Fagerholm, S., Ortegren, U., Karlsson, M., Ruishalme, I., and Strålfors, P. (2009) *PLoS ONE* **4**, e5985
7. Kublaoui, B., Lee, J., and Pilch, P. F. (1995) *J. Biol. Chem.* **270**, 59–65
8. Strålfors, P., and Honnor, R. C. (1989) *Eur. J. Biochem.* **182**, 379–385
9. Danielsson, A., Ost, A., Lystedt, E., Kjolhede, P., Gustavsson, J., Nystrom, F. H., and Strålfors, P. (2005) *FEBS J.* **272**, 141–151
10. Ortegren, U., Yin, L., Ost, A., Karlsson, H., Nystrom, F. H., and Strålfors, P. (2006) *FEBS J.* **273**, 3381–3392
11. Pettersson, T. (2008) *Global Optimization Models for Estimation of Descriptive Models*, M.Sc. thesis, Linköping University, Linköping, Sweden
12. Cedersund, G., Roll, J., Ulhhielm, E., Danielsson, A., Tidefelt, H., and Strålfors, P. (2008) *PLoS Comput. Biol.* **4**, e1000096
13. Cedersund, G., and Roll, J. (2009) *FEBS J.* **276**, 903–922
14. Kuismanen, E., and Saraste, J. (1989) *Methods Cell Biol.* **32**, 257–274
15. Thorn, H., Stenkula, K. G., Karlsson, M., Ortegren, U., Nystrom, F. H., Gustavsson, J., and Strålfors, P. (2003) *Mol. Biol. Cell* **14**, 3967–3976
16. Chen, W. W., Schoeberl, B., Jasper, P. J., Niepel, M., Nielsen, U. B., Lauffenburger, D. A., and Sorger, P. K. (2009) *Mol. Syst. Biol.* **5**, 239
17. Nahmad, M., and Stathopoulos, A. (2009) *PLoS Biol.* **7**, e1000202
18. Sedaghat, A. R., Sherman, A., and Quon, M. J. (2002) *Am. J. Physiol. Endocrinol. Metab.* **283**, E1084–E1101
19. Hori, S. S., Kurland, I. J., and DiStefano, J. J., 3rd (2006) *Ann. Biomed. Eng.* **34**, 879–892
20. Conzelmann, H., Fey, D., and Gilles, E. D. (2008) *BMC Syst. Biol.* **2**, 78
21. Borisov, N., Aksamitiene, E., Kiyatkin, A., Legewie, S., Berkhout, J., Maiwald, T., Kaimachnikov, N. P., Timmer, J., Hoek, J. B., and Kholodenko, B. N. (2009) *Mol. Syst. Biol.* **5**, 256
22. Martin, T. J., and May, J. M. (1986) *J. Recept. Res.* **6**, 323–336
23. Wanant, S., and Quon, M. J. (2000) *J. Theor. Biol.* **205**, 355–364
24. Kiselyov, V. V., Versteijhe, S., Gauguin, L., and De Meyts, P. (2009) *Mol. Syst. Biol.* **5**, 243